Regular Article

Global nonlocal viscoelastic dynamics of pulsatile fluid-conveying imperfect nanotubes

Oscar Zi Shao Ong[1], Kelly Yee[1], Ali Farajpour[1,a], Mergen H. Ghayesh[1,b], and Hamed Farokhi[2,c]

[1] School of Mechanical Engineering, University of Adelaide, South Australia 5005, Australia
[2] Department of Mechanical and Construction Engineering, Northumbria University, Newcastle upon Tyne NE1 8ST, UK

Abstract. This article aims to analyse the global nonlocal dynamics of imperfect nanoscale fluid-conveying nanotubes subject to pulsatile flow. The nanotubes are assumed to be viscoelastic. Utilising nonlocal strain gradient theory, Beskok-Karniadakis assumptions, Kelvin-Voigt scheme and Euler-Bernoulli theory, the coupled size-dependent equations are presented to account for the size effects for the nanoscale fluid and solid. Additionally, Coriolis and centrifugal accelerations, imperfection effects are considered in this article. Using different parameters, the response of the system is plotted and investigated. This investigation shows that the bifurcation response for transverse and longitudinal direction is highly dependent on the imperfection of nanotubes, the velocity and frequency of pulsatile flow. Moreover, varying different velocity components results in different responses. The preliminary results show that imperfections in fluid-conveying nanotubes reduce the chaos region.

1 Introduction

Nanotubes are largely used these days with a wide range of applications, including actuators, transistors and sensors at nanoscales [1,2]. In particular, fluid-conveying nanotubes have sparked great interest due to their variety of applications, specifically in the medical field, which includes nanopipettes, biomimetic selective transport of ions, drug delivery devices and fluid filtration devices [3–5]. Size effects play an important role in the behaviour of ultrasmall systems and structures [6–14]. A nanoscale solid, which constantly interacts with nanoscale fluid, affects the mechanical response of the system. Therefore, to be able to model the interaction of fluid with nanotube, solid-fluid interactions need to be predicted.

A plethora of literature has been done on the nonlinear dynamics and mechanical behaviour of macroscale pipes conveying fluid [15–19]. Nonetheless, the studies on the mechanical characteristics of ultrasmall pipes subject to the pulsations of a flowing fluid are limited. For macroscale structures, researchers utilise scale free formulations based on the classical continuum mechanics (CLCM), which is incapable of describing the size-dependent behaviours that an ultrasmall structure exhibits [20–23]. Therefore, to better understand the behaviour of ultrasmall structures, theoretical continuum-based models [24–27] are developed besides carrying out experimental techniques or molecular dynamics simulations. Among various theoretical modes, the modified couple stress theory (MCST) [28–33], nonlocal model [34–40] and nonlocal strain gradient theory (NSGT) [41–45] are employed for capturing size influences. In general, the MCST is utilised for microscale structures, which are governed by structural stiffness hardening, while researchers apply nonlocal modelling and NSGT to nanoscale level in which structures demonstrate stiffness softening. In this paper, the NSGT is employed for size influences.

A nonlocal elasticity theory was developed by Wang [36] for exploring the mechanics of fluid-conveying tubular ultrasmall beams; in this model, small length-scale effects were taken into consideration. Using a nonlocal elastic theory, the frequency parameters of single-walled carbon nanotube (SWCNT) conveying fluid resting on an external foundation were investigated in ref. [46]; the impacts of nonlocal stress, viscosity parameter and foundation coefficient

[a] e-mail: `ali.farajpourouderji@adelaide.edu.au` (corresponding author)
[b] e-mail: `mergen.ghayesh@adelaide.edu.au`
[c] e-mail: `hamed.farokhi@northumbria.ac.uk`

on the vibration of the nanosystem were studied. Furthermore, the oscillation features of non-uniform fluid-conveying SWCNTs resting on a viscoelastic foundation were studied by Rafiei *et al.* [47] using a non-classical formulation; the effects of scale parameters and viscoelastic foundation on the frequency and critical velocity were studied. It has been found that neglecting the scale effects would deliver inaccurate results as it has a significant impact on the mechanical features at nanoscale [9,48]. In addition, Askari and Esmailzadeh [49] implemented a non-classical beam theory for studying thermal and flow speed effects on the large-amplitude vibrations of carbon nanotubes (CNTs) conveying fluid. A nonlocal beam model was employed by Xia and Wang [50] to scrutinise the motion features of CNTs conveying fluid; CNTs were of a curved axial shape; the frequencies of curved CNTs were compared to those pf straight CNTs, and it was obtained that curved nanotubes have unconditionally high stability even at high fluid velocity. Liang and Su [51] also proposed a non-classical elasticity formulation for investigating the instability of a SWCNT conveying pulsatile flow.

In practical applications, the speed of the fluid flowing through a nanodevice would not be constant as it would be time-dependent. Besides, geometrical imperfection is likely to exist in real-world situations due to manufacturing imprecision at nanoscale levels. This initial deflection can cause significant change in the nonlinear behaviour of a nanosystem. In addition, viscosity, which models the internal energy loss due to friction, can influence the mechanical behaviour of an ultrasmall structure.

All the above-mentioned important and relevant studies on the mechanical behaviour and the nonlinear dynamics of fluid-conveying nanotubes are limited to completely perfect nanotubes with constant fluid speed. As far as is known, the simultaneous effects of imperfections coupled with flow pulsation influences on the global dynamics of viscoelastic nanotubes have not yet been studied. Therefore, this article investigates the bifurcation behaviour of imperfect viscoelastic nanotube conveying pulsatile fluid to fully understand the effects of these parameters on the nanoscale tube. By applying Hamilton's principle, coupled nonlinear equations are obtained. Then, using the approach of Galerkin's method and technique of direct integration, a reliable solution methodology is obtained for the two nonlinear equations. Subsequently, the Euler-Bernoulli strain-displacement relations are used to consider the effect of geometric imperfection of the nanotube. This is done by defining a deflection for the viscoelastic nanoscale beam along transverse axis. The effects of the fluid velocity amplitude and mean value of fluid velocity as well as the impact of geometrical imperfection on the nonlinear dynamical features of the viscoelastic nanoscale tube are explored.

2 Slip end condition

Slip conditions at the nanofluid/nanotube interface are implemented by a mathematical procedure using Karniadakis-Beskok assumptions. The fluid effective viscosity is

$$\mu_v = \left(\frac{1}{\gamma Kn + 1}\right)\mu_{v0}. \tag{1}$$

Here γ, Kn and μ_{v0} are a coefficient, Knudsen number and bulk viscosity, respectively. The appropriate value of γ is obtained as

$$\gamma = \frac{2}{\pi}\gamma_0 \tan^{-1}(\alpha_0 Kn^{\alpha_1}), \tag{2}$$

where

$$\gamma_0 = \lim_{Kn \to \infty} \gamma = \frac{64\lambda}{3\pi(\lambda - 4)}, \tag{3}$$

in which λ, α_0 and α_1 are constant values. To determine the velocity profile inside the tube, Navier-Stokes equations are employed as

$$\rho_f \frac{\mathrm{d}\boldsymbol{v}}{\mathrm{d}t} = \mu_v \nabla^2 \boldsymbol{v} - \nabla P. \tag{4}$$

Here ρ_f, $\boldsymbol{v}$ and P denote the fluid density, velocity vector and pressure, respectively. ∇^2 and ∇ represent the Laplacian and gradient operators, respectively. Using eq. (4) and assuming an incompressible laminar Newtonian fluid flow, one obtains

$$\boldsymbol{v}_x = \frac{1}{4\mu_v}\frac{\partial P}{\partial x}r^2 - \frac{R_i^2}{4\mu_v}\frac{\partial P}{\partial x}\left\{1 + \left(\frac{Kn}{\lambda Kn - 1}\right)\left(\frac{2\tau_v - 4}{\tau_v}\right)\right\}, \tag{5}$$

where R_i and τ_v indicate the inner radius of the nanotube and tangential momentum accommodation factor, respectively. Employing the above relations, the slip correction factor is obtained as

$$\kappa_{slip} = \frac{\mu_{v0}}{\mu_v}\left\{1 + \left(\frac{4Kn}{\lambda Kn - 1}\right)\left(\frac{\tau_v - 2}{\tau_v}\right)\right\}. \tag{6}$$

The above relation is utilised for simulating the impacts of slip boundary conditions at nanofluid/nanotube interfaces.
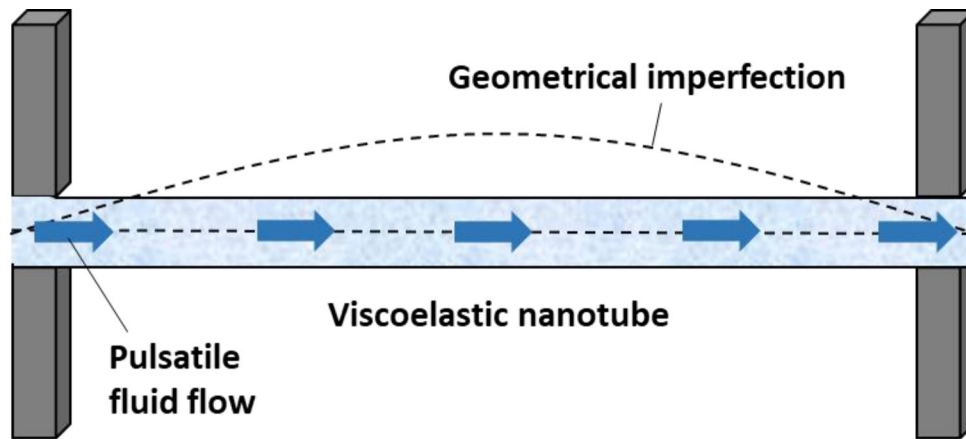
Fig. 1. A viscoelastic clamped-clamped nanotube with geometrical imperfection conveying pulsatile flow.

3 A NSGT nonlinear model for nanotubes conveying pulsatile flow

Incorporating the effects of flow pulsation, strain gradients and nonlocal stresses as well as geometrical imperfections and viscoelasticity, a nonlinear continuum model is presented in the following for the above-described problem. A thin nanoscale tube with Young's modulus E and viscosity constant η is taken into account (see fig. 1). The strain of the nanotube is

$$\varepsilon_{xx} = e_{xx} - z\kappa_{xx}, \tag{7}$$

where

$$e_{xx} = \frac{\partial u}{\partial x} + \frac{1}{2}\left(\frac{\partial w}{\partial x}\right)^2 + \frac{\partial w}{\partial x}\frac{\mathrm{d}w_0}{\mathrm{d}x}, \qquad \kappa_{xx} = \frac{\partial^2 w}{\partial x^2}, \tag{8}$$

in which w_0, w and u denote the imperfection amplitude, transverse and axial displacements, respectively. In view of the NSGT, the strain-stress equation is

$$\Gamma_{nl}\sigma_{xx} = \Gamma_{sg}\sigma_{xx(el)}^{cl} + \Gamma_{sg}\sigma_{xx(vis)}^{cl} = E\Gamma_{sg}\varepsilon_{xx} + \eta\Gamma_{sg}\frac{\partial\varepsilon_{xx}}{\partial t}, \tag{9}$$

where Γ_{nl} and Γ_{sg} are the nonlocal and strain gradient operators, respectively. In the present formulation, they are given by

$$\Gamma_{nl}(\bullet) = (\bullet) - (e_0\ell_c)^2\nabla^2(\bullet),$$
$$\Gamma_{sg}(\bullet) = (\bullet) - (\ell_{sg})^2\nabla^2(\bullet), \tag{10}$$

In eq. (10), ℓ_{sg}, ℓ_c and e_0 are the strain gradient size parameter, nonlocal size parameter and calibration coefficient, respectively. In eq. (9), "cl", "vis" and "el" as well as "sg" and "nl" are applied so as to indicate "classical", "viscoelastic" and "elastic" as well as "strain gradient" and "nonlocal", respectively. The total stress is

$$\sigma_{xx} = \sigma_{xx(el)} + \sigma_{xx(vis)}. \tag{11}$$

Assuming A as the area of cross-section, the force and moment resultants are

$$N_{xx} = \int_A \sigma_{xx}\mathrm{d}A, \qquad M_{xx} = \int_A z\sigma_{xx}\mathrm{d}A. \tag{12}$$

Using eqs. (12), (9) and (8) as well as eq. (7), one obtains

$$\Gamma_{nl}N_{xx} = EA\Gamma_{sg}\left(\frac{\partial u}{\partial x} + \frac{1}{2}\left(\frac{\partial w}{\partial x}\right)^2\right) + EA\Gamma_{sg}\left(\frac{\partial w}{\partial x}\frac{\mathrm{d}w_0}{\mathrm{d}x}\right) + \eta A\Gamma_{sg}\left(\frac{\partial^2 u}{\partial t\partial x} + \frac{\partial w}{\partial x}\frac{\partial^2 w}{\partial t\partial x}\right) + \eta A\Gamma_{sg}\left(\frac{\partial^2 w}{\partial t\partial x}\frac{\mathrm{d}w_0}{\mathrm{d}x}\right) \tag{13}$$

and

$$\Gamma_{nl}M_{xx} = -EI\Gamma_{sg}\left(\frac{\partial^2 w}{\partial x^2}\right) - \eta I\Gamma_{sg}\left(\frac{\partial^3 w}{\partial t\partial x^2}\right), \tag{14}$$

in which I is the second area moment. In view of the NSGT, the potential energy variation is

$$
\begin{aligned}
\delta U_{el} &= \int_0^L \int_A \left(\sigma_{xx(el)}^{(1)} \nabla \delta\varepsilon_{xx} + \sigma_{xx(el)}^{(0)} \delta\varepsilon_{xx} \right) \mathrm{d}A \, \mathrm{d}x \\
&= \left[\int_A \sigma_{xx(el)}^{(1)} \delta\varepsilon_{xx} \mathrm{d}A \right]_0^L + \int_0^L \int_A \left(-\nabla\sigma_{xx(el)}^{(1)} \delta\varepsilon_{xx} + \sigma_{xx(el)}^{(0)} \delta\varepsilon_{xx} \right) \mathrm{d}A \, \mathrm{d}x \\
&= \left[\int_A \sigma_{xx(el)}^{(1)} \delta\varepsilon_{xx} \mathrm{d}A \right]_0^L + \int_0^L \int_A \sigma_{xx(el)} \delta\varepsilon_{xx} \mathrm{d}A \, \mathrm{d}x.
\end{aligned}
\tag{15}
$$

Here $\sigma_{xx(el)}^{(1)}$ and $\sigma_{xx(el)}^{(0)}$ show the elastic nonlocal stresses of the first and zeroth orders, respectively. Similarly, for the viscous work variation, we have

$$
\begin{aligned}
\delta W_{vis} &= -\int_0^L \int_A \left(\sigma_{xx(vis)}^{(1)} \nabla \delta\varepsilon_{xx} + \sigma_{xx(vis)}^{(0)} \delta\varepsilon_{xx} \right) \mathrm{d}A \, \mathrm{d}x \\
&= -\left[\int_A \sigma_{xx(vis)}^{(1)} \delta\varepsilon_{xx} \mathrm{d}A \right]_0^L - \int_0^L \int_A \left(-\nabla\sigma_{xx(vis)}^{(1)} \delta\varepsilon_{xx} + \sigma_{xx(vis)}^{(0)} \delta\varepsilon_{xx} \right) \mathrm{d}A \, \mathrm{d}x \\
&= -\left[\int_A \sigma_{xx(vis)}^{(1)} \delta\varepsilon_{xx} \mathrm{d}A \right]_0^L - \int_0^L \int_A \sigma_{xx(vis)} \delta\varepsilon_{xx} \mathrm{d}A \, \mathrm{d}x.
\end{aligned}
\tag{16}
$$

In the above relation, $\sigma_{xx(vis)}^{(1)}$ and $\sigma_{xx(vis)}^{(0)}$ are the viscoelastic nonlocal stresses of the first and zeroth orders, respectively. For various stress components, one has

$$
\begin{aligned}
\sigma_{xx} &= \sigma_{xx}^{(0)} - \nabla\sigma_{xx}^{(1)}, \\
\sigma_{xx(el)} &= \sigma_{xx(el)}^{(0)} - \nabla\sigma_{xx(el)}^{(1)}, \\
\sigma_{xx(vis)} &= \sigma_{xx(vis)}^{(0)} - \nabla\sigma_{xx(vis)}^{(1)},
\end{aligned}
\tag{17}
$$

and

$$
\begin{aligned}
\sigma_{xx} &= \sigma_{xx(el)} + \sigma_{xx(vis)}, \\
\sigma_{xx}^{(0)} &= \sigma_{xx(el)}^{(0)} + \sigma_{xx(vis)}^{(0)}, \\
\sigma_{xx}^{(1)} &= \sigma_{xx(el)}^{(1)} + \sigma_{xx(vis)}^{(1)}.
\end{aligned}
\tag{18}
$$

Suppose that m and M represent (mass)/(length) for nanotube and nanofluid, respectively. Furthermore, $U(t)$ is the time-dependent fluid speed. The kinetic energy variation is

$$
\begin{aligned}
\delta T_k = {}& m \int_0^L \frac{\partial u}{\partial t} \frac{\partial \delta u}{\partial t} \mathrm{d}x + m \int_0^L \frac{\partial w}{\partial t} \frac{\partial \delta w}{\partial t} \mathrm{d}x + M \int_0^L \left(\frac{\partial u}{\partial t} + \kappa_{slip} U(t) \left(1 + \frac{\partial u}{\partial x} \right) \right) \left(\frac{\partial \delta u}{\partial t} + \kappa_{slip} U(t) \frac{\partial \delta u}{\partial x} \right) \mathrm{d}x \\
& + M \int_0^L \left(\frac{\partial w}{\partial t} + \kappa_{slip} U(t) \left(\frac{\partial w}{\partial x} + \frac{\mathrm{d}w_0}{\mathrm{d}x} \right) \right) \left(\frac{\partial \delta w}{\partial t} + \kappa_{slip} U(t) \frac{\partial \delta w}{\partial x} \right) \mathrm{d}x.
\end{aligned}
\tag{19}
$$

For the above-described nanoengineering problem, the Hamilton law, which is used for equation derivations, is expressed as

$$
\int_{t_1}^{t_2} (\delta T_k - \delta U_{el} + \delta W_{vis}) \mathrm{d}t = 0.
\tag{20}
$$

Substitution of elastic energy, viscous work and kinetic energy variations from eqs. (15), (16) and (19) into eq. (20), leads to

$$
(m+M) \frac{\partial^2 u}{\partial t^2} + M[U(t)]^2 (\kappa_{slip})^2 \frac{\partial^2 u}{\partial x^2} + \kappa_{slip} M \frac{\partial U(t)}{\partial t} \left(1 + \frac{\partial u}{\partial x} \right) + 2U(t) M \kappa_{slip} \frac{\partial^2 u}{\partial t \partial x} - \frac{\partial N_{xx}}{\partial x} = 0,
\tag{21}
$$

$$
\begin{aligned}
& (m+M) \frac{\partial^2 w}{\partial t^2} - \frac{\partial^2 M_{xx}}{\partial x^2} - \frac{\partial}{\partial x} \left[N_{xx} \left(\frac{\partial w}{\partial x} + \frac{\mathrm{d}w_0}{\mathrm{d}x} \right) \right] + 2U(t) M \kappa_{slip} \frac{\partial^2 w}{\partial t \partial x} + \kappa_{slip} M \frac{\partial U(t)}{\partial t} \left(\frac{\partial w}{\partial x} + \frac{\mathrm{d}w_0}{\mathrm{d}x} \right) \\
& + M[U(t)]^2 (\kappa_{slip})^2 \left(\frac{\partial^2 w}{\partial x^2} + \frac{\mathrm{d}^2 w_0}{\mathrm{d}x^2} \right) = 0.
\end{aligned}
\tag{22}
$$

It is worth mentioning that when the slip correction factor is set to 1, eqs. (21) and (22) are reduced to those of no-slip boundary conditions. Applying eqs. (21) and (22) as well as eqs. (13) and (14), moment and force resultants are obtained as

$$
N_{xx} = EA\Gamma_{sg}\left(\frac{\partial u}{\partial x} + \frac{1}{2}\left(\frac{\partial w}{\partial x}\right)^2\right) + EA\Gamma_{sg}\left(\frac{\partial w}{\partial x}\frac{\mathrm{d}w_0}{\mathrm{d}x}\right)
$$

$$
+ \eta A\Gamma_{sg}\left(\frac{\partial^2 u}{\partial t\partial x} + \frac{\partial w}{\partial x}\frac{\partial^2 w}{\partial t\partial x}\right) + \eta A\Gamma_{sg}\left(\frac{\partial^2 w}{\partial t\partial x}\frac{\mathrm{d}w_0}{\mathrm{d}x}\right)
$$

$$
+ (e_0\ell_c)^2\left\{(m+M)\frac{\partial^3 u}{\partial x\partial t^2} + 2U(t)M\kappa_{slip}\frac{\partial^3 u}{\partial t\partial x^2}\right.
$$

$$
\left. + M[U(t)]^2(\kappa_{slip})^2\frac{\partial^3 u}{\partial x^3} + \kappa_{slip}M\frac{\partial U(t)}{\partial t}\frac{\partial^2 u}{\partial x^2}\right\},
\tag{23}
$$

$$
M_{xx} = -EI\Gamma_{sg}\frac{\partial^2 w}{\partial x^2} - \eta I\Gamma_{sg}\frac{\partial^3 w}{\partial t\partial x^2} - (e_0\ell_c)^2\frac{\partial}{\partial x}\left[N_{xx}\left(\frac{\partial w}{\partial x} + \frac{\mathrm{d}w_0}{\mathrm{d}x}\right)\right]
$$

$$
+ (e_0\ell_c)^2\left\{(m+M)\frac{\partial^2 w}{\partial t^2} + M[U(t)]^2(\kappa_{slip})^2\left(\frac{\partial^2 w}{\partial x^2} + \frac{\mathrm{d}^2 w_0}{\mathrm{d}x^2}\right)\right.
$$

$$
\left. + 2U(t)M\kappa_{slip}\frac{\partial^2 w}{\partial t\partial x} + \kappa_{slip}M\left(\frac{\partial w}{\partial x} + \frac{\mathrm{d}w_0}{\mathrm{d}x}\right)\frac{\partial U(t)}{\partial t}\right\}.
\tag{24}
$$

Substitution of eqs. (23) and (24) into eqs. (21) and (22), assuming the fluid speed as $U = U_0 + U_1\cos(\omega_f t)$, and then using the following dimensionless parameters:

$$
\xi = \frac{x}{L}, \qquad \bar{\nabla}^2 = \frac{\partial^2}{\partial\xi^2}, \qquad \chi_{nl} = \frac{e_0\ell_c}{L},
$$

$$
\chi_{sg} = \frac{\ell_{sg}}{L}, \qquad u^* = \frac{u}{d}, \qquad w_0^* = \frac{w_0}{d},
$$

$$
w^* = \frac{w}{d}, \qquad \Xi = \frac{AL^2}{I}, \qquad s = \frac{L}{d},
$$

$$
\bar{M} = \frac{M}{M+m}, \qquad t^* = \frac{t}{L^2}\sqrt{\frac{EI}{m+M}}, \qquad U^* = \sqrt{\frac{M}{EI}}UL,
$$

$$
\omega^* = \sqrt{\frac{L^4(m+M)}{EI}}\omega, \qquad \eta^* = \sqrt{\frac{EI}{m+M}}\frac{\eta}{EL^2},
\tag{25}
$$

the dimensionless motion equations, which are both nonlinear and viscoelastically coupled, are derived as

$$
\frac{s}{\Xi}\left\{\frac{\partial^2 u}{\partial t^2} + 2\sqrt{\bar{M}}\kappa_{slip}\frac{\partial^2 u}{\partial t\partial\xi}[U_0 + U_1\cos(\omega_f t)] + (\kappa_{slip})^2\frac{\partial^2 u}{\partial\xi^2}[U_0 + U_1\cos(\omega_f t)]^2 - \kappa_{slip}\omega_f\sqrt{\bar{M}}U_1\left(s + \frac{\partial u}{\partial\xi}\right)\sin(\omega_f t)\right\}
$$

$$
- \chi_{nl}^2\frac{s}{\Xi}\frac{\partial^2}{\partial\xi^2}\left\{\frac{\partial^2 u}{\partial t^2} + 2\sqrt{\bar{M}}\kappa_{slip}\frac{\partial^2 u}{\partial t\partial\xi}[U_0 + U_1\cos(\omega_f t)] + (\kappa_{slip})^2\frac{\partial^2 u}{\partial\xi^2}[U_0 + U_1\cos(\omega_f t)]^2\right.
$$

$$
\left. - \kappa_{slip}\omega_f\sqrt{\bar{M}}U_1\left(s + \frac{\partial u}{\partial\xi}\right)\sin(\omega_f t)\right\} - \frac{\partial}{\partial\xi}\left[s\frac{\partial u}{\partial\xi} + \frac{1}{2}\left(\frac{\partial w}{\partial\xi}\right)^2 + \frac{\partial w}{\partial\xi}\frac{\mathrm{d}w_0}{\mathrm{d}\xi}\right] + \chi_{sg}^2\frac{\partial^3}{\partial\xi^3}\left[s\frac{\partial u}{\partial\xi} + \frac{1}{2}\left(\frac{\partial w}{\partial\xi}\right)^2 + \frac{\partial w}{\partial\xi}\frac{\mathrm{d}w_0}{\mathrm{d}\xi}\right]
$$

$$
- \eta\frac{\partial}{\partial\xi}\left(s\frac{\partial^2 u}{\partial t\partial\xi} + \frac{\partial w}{\partial\xi}\frac{\partial^2 w}{\partial t\partial\xi} + \frac{\partial^2 w}{\partial t\partial\xi}\frac{\mathrm{d}w_0}{\mathrm{d}\xi}\right) + \chi_{sg}^2\eta\frac{\partial^3}{\partial\xi^3}\left(s\frac{\partial^2 u}{\partial t\partial\xi} + \frac{\partial w}{\partial\xi}\frac{\partial^2 w}{\partial t\partial\xi} + \frac{\partial^2 w}{\partial t\partial\xi}\frac{\mathrm{d}w_0}{\mathrm{d}\xi}\right) = 0,
\tag{26}
$$

$$
\frac{\partial^2 w}{\partial t^2} + 2\kappa_{slip}\sqrt{\bar{M}}\frac{\partial^2 w}{\partial t\partial \xi}[U_0 + U_1\cos(\omega_f t)] + (\kappa_{slip})^2\left(\frac{\partial^2 w}{\partial \xi^2} + \frac{\mathrm{d}^2 w_0}{\mathrm{d}\xi^2}\right)[U_0 + U_1\cos(\omega_f t)]^2
$$

$$
- \kappa_{slip}\omega_f\sqrt{\bar{M}}U_1\left(\frac{\partial w}{\partial \xi} + \frac{\mathrm{d}w_0}{\mathrm{d}\xi}\right)\sin(\omega_f t) - \chi_{nl}^2\frac{\partial^2}{\partial \xi^2}\left\{\frac{\partial^2 w}{\partial t^2} + 2\sqrt{\bar{M}}\kappa_{slip}\frac{\partial^2 w}{\partial t\partial \xi}[U_0 + U_1\cos(\omega_f t)]\right.
$$

$$
+ (\kappa_{slip})^2\left(\frac{\partial^2 w}{\partial \xi^2} + \frac{\mathrm{d}^2 w_0}{\mathrm{d}\xi^2}\right)[U_0 + U_1\cos(\omega_f t)]^2 - \kappa_{slip}\omega_f\sqrt{\bar{M}}U_1\left(\frac{\partial w}{\partial \xi} + \frac{\mathrm{d}w_0}{\mathrm{d}\xi}\right)\sin(\omega_f t)\Bigg\}
$$

$$
+ \frac{\partial^4 w}{\partial \xi^4} - \chi_{sg}^2\frac{\partial^6 w}{\partial \xi^6} + \eta\frac{\partial^5 w}{\partial t\partial \xi^4} - \chi_{sg}^2\eta\frac{\partial^7 w}{\partial t\partial \xi^6} - \frac{\Xi}{s^2}\frac{\partial}{\partial \xi}\left\{\left(\frac{\partial w}{\partial \xi} + \frac{\mathrm{d}w_0}{\mathrm{d}\xi}\right)\left[s\frac{\partial u}{\partial \xi} + \frac{1}{2}\left(\frac{\partial w}{\partial \xi}\right)^2 + \frac{\partial w}{\partial \xi}\frac{\mathrm{d}w_0}{\mathrm{d}\xi}\right]\right.
$$

$$
- \chi_{sg}^2\left(\frac{\partial w}{\partial \xi} + \frac{\mathrm{d}w_0}{\mathrm{d}\xi}\right)\frac{\partial^2}{\partial \xi^2}\left[s\frac{\partial u}{\partial \xi} + \frac{1}{2}\left(\frac{\partial w}{\partial \xi}\right)^2 + \frac{\partial w}{\partial \xi}\frac{\mathrm{d}w_0}{\mathrm{d}\xi}\right] + \eta\left(\frac{\partial w}{\partial \xi} + \frac{\mathrm{d}w_0}{\mathrm{d}\xi}\right)\left(s\frac{\partial^2 u}{\partial t\partial \xi} + \frac{\partial w}{\partial \xi}\frac{\partial^2 w}{\partial t\partial \xi} + \frac{\partial^2 w}{\partial t\partial \xi}\frac{\mathrm{d}w_0}{\mathrm{d}\xi}\right)
$$

$$
- \chi_{sg}^2\eta\left(\frac{\partial w}{\partial \xi} + \frac{\mathrm{d}w_0}{\mathrm{d}\xi}\right)\frac{\partial^2}{\partial \xi^2}\left(s\frac{\partial^2 u}{\partial t\partial \xi} + \frac{\partial w}{\partial \xi}\frac{\partial^2 w}{\partial t\partial \xi} + \frac{\partial^2 w}{\partial t\partial \xi}\frac{\mathrm{d}w_0}{\mathrm{d}\xi}\right) + \frac{s}{\Xi}\chi_{nl}^2\left(\frac{\partial w}{\partial \xi} + \frac{\mathrm{d}w_0}{\mathrm{d}\xi}\right)
$$

$$
\times\left(\frac{\partial^3 u}{\partial \xi\partial t^2} + 2\sqrt{\bar{M}}\kappa_{slip}\frac{\partial^3 u}{\partial t\partial \xi^2}[U_0 + U_1\cos(\omega_f t)] + (\kappa_{slip})^2\frac{\partial^3 u}{\partial \xi^3}[U_0 + U_1\cos(\omega_f t)]^2 - \kappa_{slip}\omega_f\sqrt{\bar{M}}U_1\frac{\partial^2 u}{\partial \xi^2}\sin(\omega_f t)\right)\Bigg\}
$$

$$
+ \frac{\Xi}{s^2}\chi_{nl}^2\frac{\partial^3}{\partial \xi^3}\left\{\left(\frac{\partial w}{\partial \xi} + \frac{\mathrm{d}w_0}{\mathrm{d}\xi}\right)\left[s\frac{\partial u}{\partial \xi} + \frac{1}{2}\left(\frac{\partial w}{\partial \xi}\right)^2 + \frac{\partial w}{\partial \xi}\frac{\mathrm{d}w_0}{\mathrm{d}\xi}\right] - \chi_{sg}^2\left(\frac{\partial w}{\partial \xi} + \frac{\mathrm{d}w_0}{\mathrm{d}\xi}\right)\frac{\partial^2}{\partial \xi^2}\left[s\frac{\partial u}{\partial \xi} + \frac{1}{2}\left(\frac{\partial w}{\partial \xi}\right)^2 + \frac{\partial w}{\partial \xi}\frac{\mathrm{d}w_0}{\mathrm{d}\xi}\right]\right.
$$

$$
+ \eta\left(\frac{\partial w}{\partial \xi} + \frac{\mathrm{d}w_0}{\mathrm{d}\xi}\right)\left(s\frac{\partial^2 u}{\partial t\partial \xi} + \frac{\partial w}{\partial \xi}\frac{\partial^2 w}{\partial t\partial \xi} + \frac{\partial^2 w}{\partial t\partial \xi}\frac{\mathrm{d}w_0}{\mathrm{d}\xi}\right) - \eta\chi_{sg}^2\left(\frac{\partial w}{\partial \xi} + \frac{\mathrm{d}w_0}{\mathrm{d}\xi}\right)\frac{\partial^2}{\partial \xi^2}\left(s\frac{\partial^2 u}{\partial t\partial \xi} + \frac{\partial w}{\partial \xi}\frac{\partial^2 w}{\partial t\partial \xi} + \frac{\partial^2 w}{\partial t\partial \xi}\frac{\mathrm{d}w_0}{\mathrm{d}\xi}\right)
$$

$$
+ \chi_{nl}^2\frac{s}{\Xi}\left(\frac{\partial w}{\partial \xi} + \frac{\mathrm{d}w_0}{\mathrm{d}\xi}\right)\left(\frac{\partial^3 u}{\partial \xi\partial t^2} + 2\sqrt{\bar{M}}\kappa_{slip}\frac{\partial^3 u}{\partial t\partial \xi^2}[U_0 + U_1\cos(\omega_f t)]\right.
$$

$$
+ (\kappa_{slip})^2\frac{\partial^3 u}{\partial \xi^3}[U_0 + U_1\cos(\omega_f t)]^2 - \kappa_{slip}\omega_f\sqrt{\bar{M}}U_1\frac{\partial^2 u}{\partial \xi^2}\sin(\omega_f t)\bigg)\Bigg\} = 0. \tag{27}
$$

4 Numerical solution

Firstly, for convenience purposes, the nonlinear coupled motion equations are re-written using the following set of differential operators:

$$
\Upsilon_{1,1}(\bullet) = \frac{\partial^2}{\partial t^2}(\bullet) + 2\sqrt{\bar{M}}\kappa_{slip}[U_0 + U_1\cos(\omega_f t)]\frac{\partial^2(\bullet)}{\partial t\partial \xi}
$$

$$
+ (\kappa_{slip})^2[U_0 + U_1\cos(\omega_f t)]^2\frac{\partial^2}{\partial \xi^2}(\bullet) - \kappa_{slip}\omega_f\sqrt{\bar{M}}U_1\sin(\omega_f t)\left(s + \frac{\partial}{\partial \xi}(\bullet)\right),
$$

$$
\Upsilon_{1,2}(\bullet, *, \circ) = s\frac{\partial}{\partial \xi}(\bullet) + \frac{1}{2}\left(\frac{\partial}{\partial \xi}(*)\right)^2 + \left[\frac{\partial}{\partial \xi}(*)\right]\left[\frac{\mathrm{d}}{\mathrm{d}\xi}(\circ)\right],
$$

$$
\Upsilon_{1,3}(\bullet, *, \circ) = s\frac{\partial^2}{\partial t\partial \xi}(\bullet) + \left[\frac{\partial}{\partial \xi}(*)\right]\left[\frac{\partial^2}{\partial t\partial \xi}(*)\right] + \left[\frac{\partial^2}{\partial t\partial \xi}(*)\right]\left[\frac{\mathrm{d}}{\mathrm{d}\xi}(\circ)\right], \tag{28}
$$

$$
\Upsilon_{2,1}(\bullet, \circ) = \frac{\partial^2}{\partial t^2}(\bullet) + 2\sqrt{\bar{M}}\kappa_{slip}[U_0 + U_1\cos(\omega_f t)]\frac{\partial^2(\bullet)}{\partial t\partial \xi} + (\kappa_{slip})^2[U_0 + U_1\cos(\omega_f t)]^2\left[\frac{\partial^2}{\partial \xi^2}(\bullet) + \frac{\partial^2}{\partial \xi^2}(\circ)\right]
$$

$$
- \kappa_{slip}\omega_f\sqrt{\bar{M}}U_1\sin(\omega_f t)\left[\frac{\partial}{\partial \xi}(\bullet) + \frac{\partial}{\partial \xi}(\circ)\right],
$$

$$
\Upsilon_{2,2}(\bullet) = \frac{\partial^4}{\partial \xi^4}(\bullet) - \chi_{sg}^2\frac{\partial^6}{\partial \xi^6}(\bullet) + \eta\frac{\partial^5}{\partial t\partial \xi^4}(\bullet) - \chi_{sg}^2\eta\frac{\partial^7}{\partial t\partial \xi^6}(\bullet),
$$

$$
\Upsilon_{2,3}(\bullet, \circ) = \frac{\partial}{\partial \xi}(\bullet) + \frac{\partial}{\partial \xi}(\circ),
$$

$$
\Upsilon_{2,4}(\bullet) = \frac{\partial^3}{\partial \xi\partial t^2}(\bullet) + 2\sqrt{\bar{M}}\kappa_{slip}[U_0 + U_1\cos(\omega_f t)]\frac{\partial^3}{\partial t\partial \xi^2}(\bullet)
$$

$$
+ (\kappa_{slip})^2[U_0 + U_1\cos(\omega_f t)]^2\frac{\partial^3}{\partial \xi^3}(\bullet) - \kappa_{slip}\omega_f\sqrt{\bar{M}}U_1\sin(\omega_f t)\frac{\partial^2}{\partial \xi^2}(\bullet). \tag{29}
$$

Using the above differential operators, eqs. (26) and (27) are re-written as follows:

$$\frac{s}{\Xi}\Upsilon_{1,1}(u) - \chi_{nl}^2\frac{s}{\Xi}\frac{\partial^2}{\partial\xi^2}[\Upsilon_{1,1}(u)] - \frac{\partial}{\partial\xi}[\Upsilon_{1,2}(u,w,w_0)]$$

$$+ \chi_{sg}^2\frac{\partial^3}{\partial\xi^3}[\Upsilon_{1,2}(u,w,w_0)] - \eta\frac{\partial}{\partial\xi}[\Upsilon_{1,3}(u,w,w_0)] + \chi_{sg}^2\eta\frac{\partial^3}{\partial\xi^3}[\Upsilon_{1,3}(u,w,w_0)] = 0, \tag{30}$$

$$\Upsilon_{2,1}(w,w_0) + \Upsilon_{2,2}(w) - \chi_{nl}^2\frac{\partial^2}{\partial\xi^2}[\Upsilon_{2,1}(w,w_0)]$$

$$- \frac{\Xi}{s^2}\frac{\partial}{\partial\xi}\Bigg\{[\Upsilon_{1,2}(u,w,w_0)][\Upsilon_{2,3}(w,w_0)] - \chi_{sg}^2[\Upsilon_{2,3}(w,w_0)]\frac{\partial^2}{\partial\xi^2}[\Upsilon_{1,2}(u,w,w_0)] + \eta[\Upsilon_{2,3}(w,w_0)]\Upsilon_{1,3}(u,w,w_0)$$

$$- \chi_{sg}^2\eta[\Upsilon_{2,3}(w,w_0)]\frac{\partial^2}{\partial\xi^2}[\Upsilon_{1,3}(u,w,w_0)] + \frac{s}{\Xi}\chi_{nl}^2[\Upsilon_{2,3}(w,w_0)]\Upsilon_{2,4}(u)\Bigg\}$$

$$+ \frac{\Xi}{s^2}\chi_{nl}^2\frac{\partial^3}{\partial\xi^3}\Bigg\{\Upsilon_{2,3}(w,w_0)\Upsilon_{1,2}(u,w,w_0) - \chi_{sg}^2\Upsilon_{2,3}(w,w_0)\frac{\partial^2}{\partial\xi^2}[\Upsilon_{1,2}(u,w,w_0)] + \eta\Upsilon_{2,3}(w,w_0)\Upsilon_{1,3}(u,w,w_0)$$

$$- \eta\chi_{sg}^2\Upsilon_{2,3}(w,w_0)\frac{\partial^2}{\partial\xi^2}[\Upsilon_{1,3}(u,w,w_0)] + \chi_{nl}^2\frac{s}{\Xi}\Upsilon_{2,3}(w,w_0)\Upsilon_{2,4}(u)\Bigg\} = 0. \tag{31}$$

Now the simplified nonlinear coupled equations are discretised via application of a weighted-residual technique [52–55]. Assuming both ends of the tube as clamped ends, the axial and transverse components of the displacement field are

$$u(t,\xi) = \sum_{k=1}^{N_u} p_k(t)\Phi_k(\xi),$$

$$w(t,\xi) = \sum_{k=1}^{N_w} q_k(t)\Psi_k(\xi), \tag{32}$$

where (p,q) and (Φ,Ψ) stand for the generalised coordinates and basis functions, respectively, [56,57]. N_i $(i = u,w)$ is also employed to show the number of generalised coordinates. Substitution of eq. (32) into eqs. (30) and (31), then implementing Galerkin's scheme, yields

$$\int_0^1 \Phi_j(\xi)\Bigg\{\frac{s}{\Xi}\Upsilon_{1,1}\left(\sum_{k=1}^{N_u} p_k(t)\Phi_k(\xi)\right) - \chi_{nl}^2\frac{s}{\Xi}\left[\Upsilon_{1,1}\left(\sum_{k=1}^{N_u}\Phi_k(\xi)p_k(t)\right)\right]''$$

$$- \left[\Upsilon_{1,2}\left(\sum_{k=1}^{N_u}\Phi_k(\xi)p_k(t), \sum_{k=1}^{N_u}\Psi_k(\xi)q_k(t), A_0\Psi_1(\xi)\right)\right]'$$

$$+ \chi_{sg}^2\left[\Upsilon_{1,2}\left(\sum_{k=1}^{N_u}\Phi_k(\xi)p_k(t), \sum_{k=1}^{N_u}\Psi_k(\xi)q_k(t), A_0\Psi_1(\xi)\right)\right]'''$$

$$- \eta\left[\Upsilon_{1,3}\left(\sum_{k=1}^{N_u}\Phi_k(\xi)p_k(t), \sum_{k=1}^{N_u}\Psi_k(\xi)q_k(t), A_0\Psi_1(\xi)\right)\right]'$$

$$+ \chi_{sg}^2\eta\left[\Upsilon_{1,3}\left(\sum_{k=1}^{N_u}\Phi_k(\xi)p_k(t), \sum_{k=1}^{N_u}\Psi_k(\xi)q_k(t), A_0\Psi_1(\xi)\right)\right]'''\Bigg\}\mathrm{d}\xi = 0, \tag{33}$$

$$\int_0^1 \Psi_j(\xi) \Bigg\{ \Upsilon_{2,1}\left(\sum_{k=1}^{N_u} q_k(t)\Psi_k(\xi), A_0\Psi_1(\xi)\right)$$

$$- \chi_{nl}^2\left[\Upsilon_{2,1}\left(\sum_{k=1}^{N_u} q_k(t)\Psi_k(\xi), A_0\Psi_1(\xi)\right)\right]'' + \Upsilon_{2,2}\left(\sum_{k=1}^{N_u} q_k(t)\Psi_k(\xi)\right)$$

$$- \frac{\Xi}{s^2}\Bigg\{\left[\Upsilon_{2,3}\left(\sum_{k=1}^{N_u} q_k(t)\Psi_k(\xi), A_0\Psi_1(\xi)\right)\right]\left[\Upsilon_{1,2}\left(\sum_{k=1}^{N_u} \Phi_k(\xi)p_k(t), \sum_{k=1}^{N_u}\Psi_k(\xi)q_k(t), A_0\Psi_1(\xi)\right)\right]$$

$$- \chi_{sg}^2\left[\Upsilon_{2,3}\left(\sum_{k=1}^{N_u} q_k(t)\Psi_k(\xi), A_0\Psi_1(\xi)\right)\right]\left(\left[\Upsilon_{1,2}\left(\sum_{k=1}^{N_u} p_k(t)\Phi_k(\xi), \sum_{k=1}^{N_u}q_k(t)\Psi_k(\xi), A_0\Psi_1(\xi)\right)\right]''\right)$$

$$+ \eta\left[\Upsilon_{2,3}\left(\sum_{k=1}^{N_u} q_k(t)\Psi_k(\xi), A_0\Psi_1(\xi)\right)\right]\left[\Upsilon_{1,3}\left(\sum_{k=1}^{N_u} \Phi_k(\xi)p_k(t), \sum_{k=1}^{N_u}\Psi_k(\xi)q_k(t), A_0\Psi_1(\xi)\right)\right]$$

$$- \chi_{sg}^2\eta\left[\Upsilon_{2,3}\left(\sum_{k=1}^{N_u} \Psi_k(\xi)q_k(t), A_0\Psi_1(\xi)\right)\right]\left(\left[\Upsilon_{1,3}\left(\sum_{k=1}^{N_u} p_k(t)\Phi_k(\xi), \sum_{k=1}^{N_u}q_k(t)\Psi_k(\xi), A_0\Psi_1(\xi)\right)\right]''\right)$$

$$+ \frac{s}{\Xi}\chi_{nl}^2\left[\Upsilon_{2,3}\left(\sum_{k=1}^{N_u} \Psi_k(\xi)q_k(t), A_0\Psi_1(\xi)\right)\right]\Upsilon_{2,4}\left(\sum_{k=1}^{N_u} \Phi_k(\xi)p_k(t)\right)\Bigg\}'$$

$$+ \frac{\Xi}{s^2}\chi_{nl}^2\Bigg\{\left[\Upsilon_{2,3}\left(\sum_{k=1}^{N_u} \Psi_k(\xi)q_k(t), A_0\Psi_1(\xi)\right)\right]\left[\Upsilon_{1,2}\left(\sum_{k=1}^{N_u} \Phi_k(\xi)p_k(t), \sum_{k=1}^{N_u}\Psi_k(\xi)q_k(t), A_0\Psi_1(\xi)\right)\right]$$

$$- \chi_{sg}^2\left[\Upsilon_{2,3}\left(\sum_{k=1}^{N_u} q_k(t)\Psi_k(\xi), A_0\Psi_1(\xi)\right)\right]\left(\left[\Upsilon_{1,2}\left(\sum_{k=1}^{N_u} p_k(t)\Phi_k(\xi), \sum_{k=1}^{N_u}\Psi_k(\xi)q_k(t), A_0\Psi_1(\xi)\right)\right]''\right)$$

$$+ \eta\left[\Upsilon_{2,3}\left(\sum_{k=1}^{N_u} \Psi_k(\xi)q_k(t), A_0\Psi_1(\xi)\right)\right]\left[\Upsilon_{1,3}\left(\sum_{k=1}^{N_u} p_k(t)\Phi_k(\xi), \sum_{k=1}^{N_u}\Psi_k(\xi)q_k(t), A_0\Psi_1(\xi)\right)\right]$$

$$- \eta\chi_{sg}^2\left[\Upsilon_{2,3}\left(\sum_{k=1}^{N_u} \Psi_k(\xi)q_k(t), A_0\Psi_1(\xi)\right)\right]\left(\left[\Upsilon_{1,3}\left(\sum_{k=1}^{N_u} p_k(t)\Phi_k(\xi), \sum_{k=1}^{N_u}\Psi_k(\xi)q_k(t), A_0\Psi_1(\xi)\right)\right]''\right)$$

$$+ \chi_{nl}^2\frac{s}{\Xi}\Upsilon_{2,3}\left(\sum_{k=1}^{N_u} q_k(t)\Psi_k(\xi), A_0\Psi_1(\xi)\right)\Upsilon_{2,4}\left(\sum_{k=1}^{N_u} \Phi_k(\xi)p_k(t)\right)\Bigg\}'''\Bigg\}\mathrm{d}\xi = 0. \tag{34}$$

Finally, to determine the global nonlocal viscoelastic dynamic characteristics of fluid-conveying imperfect nanotubes with flow pulsation, a technique of direct integration is implemented. It should be noticed that the number of generalised coordinates along the x-axis is assumed to be the same as that of the z-axis.

5 Numerical results

A nanoscale tube, which is utilised as an ultrasmall device to convey pulsatile fluid, is taken into account. For the solid part, we assume that $E = 610\,\mathrm{MPa}$, Poisson's ratio $= 0.3$, density $= 1024\,\mathrm{kg/m^3}$, outer radius $= 290.5\,\mathrm{nm}$, thickness $= 66.0\,\mathrm{nm}$ and $s = 20$. The Knudsen number, dimensionless fluid mass and slip correction factor are $Kn = 0.015$, $\bar{M} = 0.5915$ and $\kappa_{slip} = 1.119$, respectively. Furthermore, it is assumed that $\Xi = 4006.94$, $\eta^* = 0.0004$, $\chi_{sg} = 0.04$ and $\chi_{nl} = 0.08$. In numerical calculation, 20 degrees of freedom are considered. In addition, the coefficient associated with slip boundary conditions are taken as $\lambda = -1$, $\tau_v = 0.7$, $\alpha_0 = 4$, $\alpha_1 = 0.4$ and $\gamma_0 = 64/(15\pi)$ in this nonlinear dynamical analysis.

The static bifurcation response is first plotted in figs. 2, varying A_0 from 0.005 to 0.05. This shows the relationship between U_0 and the resultant transverse deflection at $x = 0.50$. From the figure, it is observed that the system remains unchanged till U_0 reaches a certain speed where the system starts to deflect. For the system where $A_0 = 0.005$, the speed is 4.8 and the effect of the speed is evident in figs. 3 when the pulsatile fluid is introduced, $(U_1 = 0.05U_0)$. Comparing the transverse deflection of the nanobeam as U_0 exceeds the critical speed when $A_0 = 0.005$, it can be seen
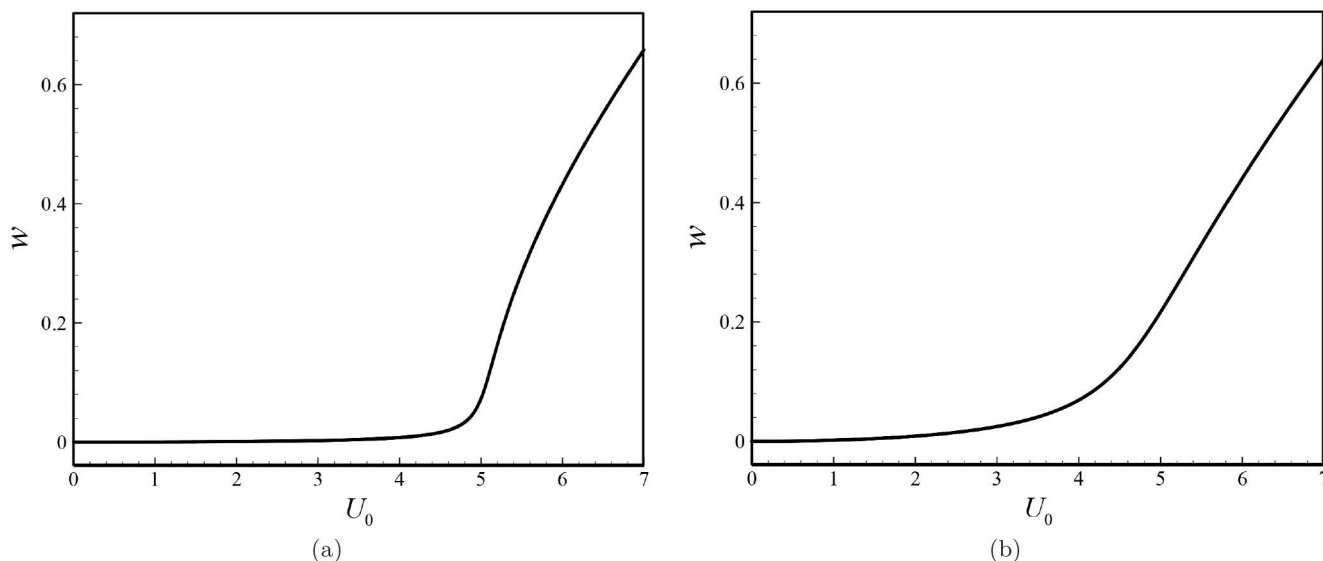
Fig. 2. Static bifurcations of initially imperfect nanofluid-conveying nanotubes showing the transverse deflection at $x = 0.50$ for $U_1 = 0$: (a) $A_0 = 0.005$; (b) $A_0 = 0.05$.
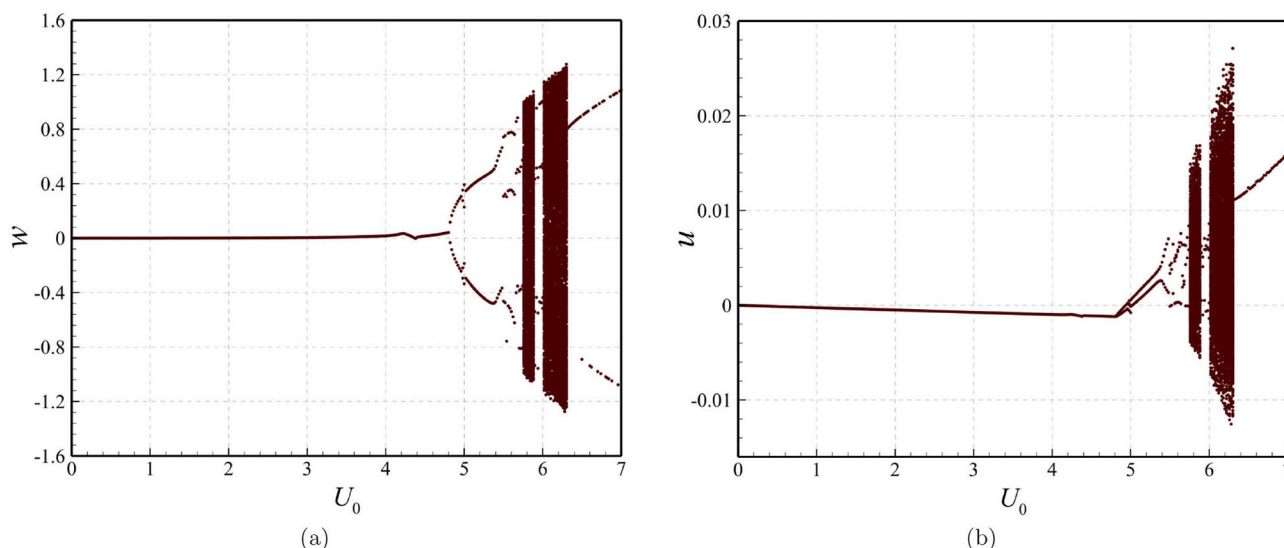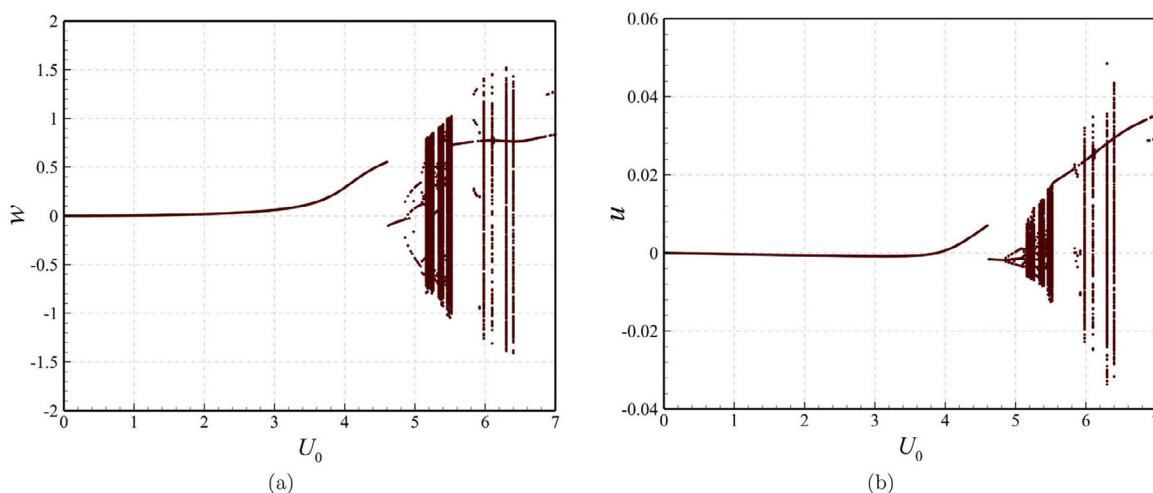

Fig. 3. Bifurcation response of initially imperfect nanofluid-conveying viscoelastic nanotubes for $A_0 = 0.005$, $\omega_f = 10.50$, and $U_1 = 0.05U_0$: (a) $w[x = 0.50]$; (b) $u[x = 0.65]$.

the coupled motion after $U_0 = 4.8$, increases from period-1 to period-2 and the motion is unpredictable after that. It is also observed that period-3 coupled motion is seen after $U_0 = 5.5$, and it is complete chaos starting at $U_0 = 5.76$. To be able to understand more about the chaotic motion, more detailed plots at $U_0 = 6.3$ are shown in figs. 4. It is worth noting that the pattern of motion cannot be predicted over time.

Figure 5 demonstrates the bifurcation response when the system has a higher imperfection ($A_0 = 0.05$). ω_f is increased from 10.50 to 12, and the speed of U_1 is increased to $0.10U_0$. Different motion types can be observed in these figures. The system's transverse motion response is similar to the static bifurcation shown in fig. 1 but with larger amplitude until $U_0 = 4.6$. The coupled motion is periodic for $0 < U_0 < 4.84$, a mixture of period-2 and period-1 as well as period-3 motion is seen for $4.86 < U_0 < 5.08$, after that it is observed to be chaos. Numerous period-1 motions are found for $5.54 < U_0 < 6.6$ in between intervals. For example, it is observed that chaos happens when $U_0 = 6.3$ and the system returns to a period-1 motion after that, and again chaos happens when $U_0 = 6.4$. However, it is noted that a system with higher imperfections shows more intervals of chaos. To be able to observe the periodic motion more clearly, fig. 6 is plotted to show the variation of transverse and longitudinal motion at $U_0 = 4.6$ as time varies. For further clarification, the chaotic motion at $U_0 = 5.5$ is plotted in fig. 7. From the figure, it is observed that the system experiences chaotic motions where a pattern cannot be spotted in transverse and longitudinal directions.
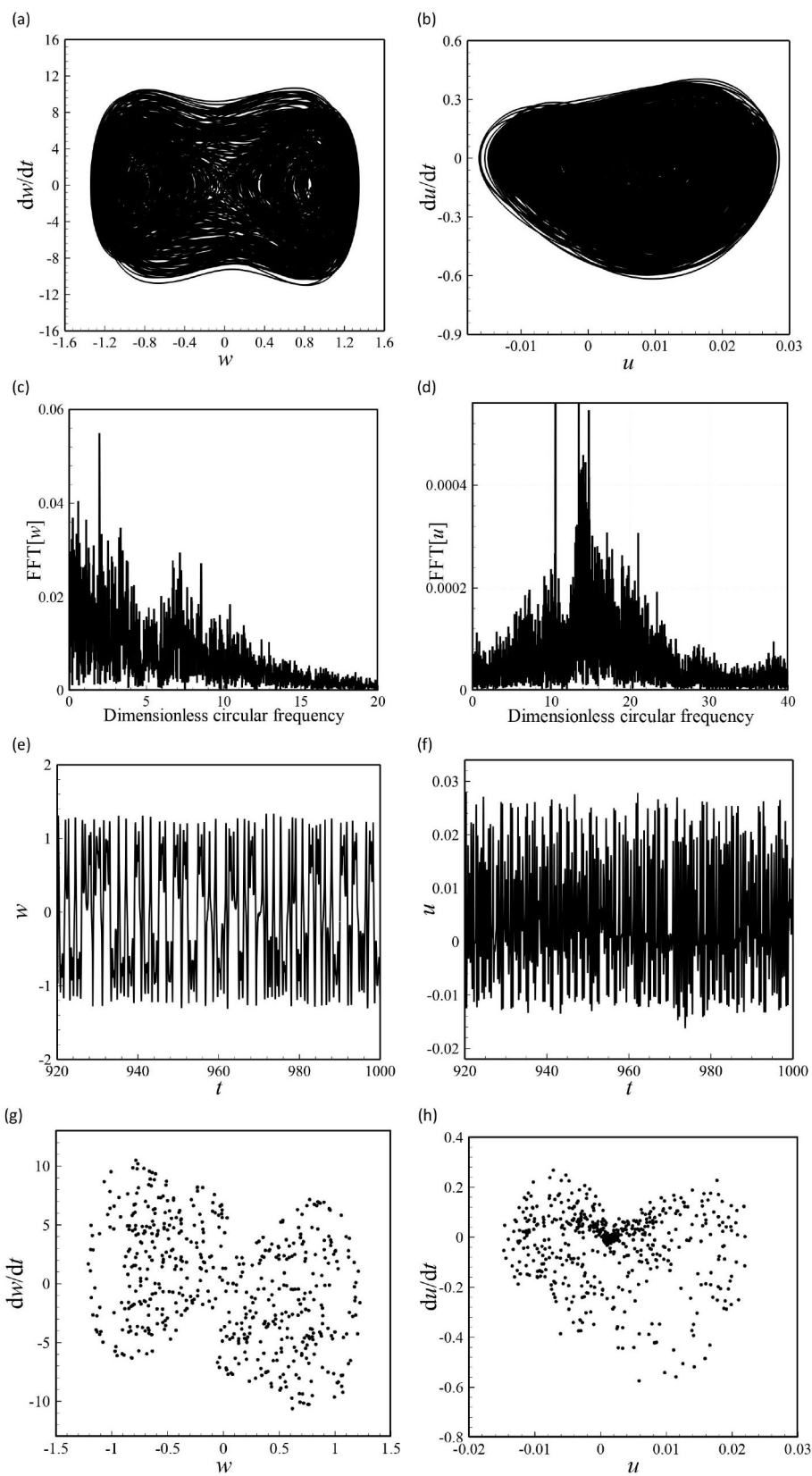
Fig. 4. Response of the tube in fig. 3 at $U_0 = 6.30$ for $A_0 = 0.005$, $\omega_f = 10.50$, and $U_1 = 0.05U_0$: (a), (c), (e), and (g) phase-plane, FFT, time trace, and Poincaré sections for $w[x = 0.5]$, respectively; (b), (d), (f), and (h) phase-plane, FFT, time trace, and Poincaré sections for $u[x = 0.65]$, respectively.

Fig. 5. Bifurcation response of initially imperfect nanofluid-conveying viscoelastic nanotubes for $A_0 = 0.05$, $\omega_f = 12.00$, and $U_1 = 0.10U_0$: (a) $w[x = 0.50]$; (b) $u[x = 0.65]$.
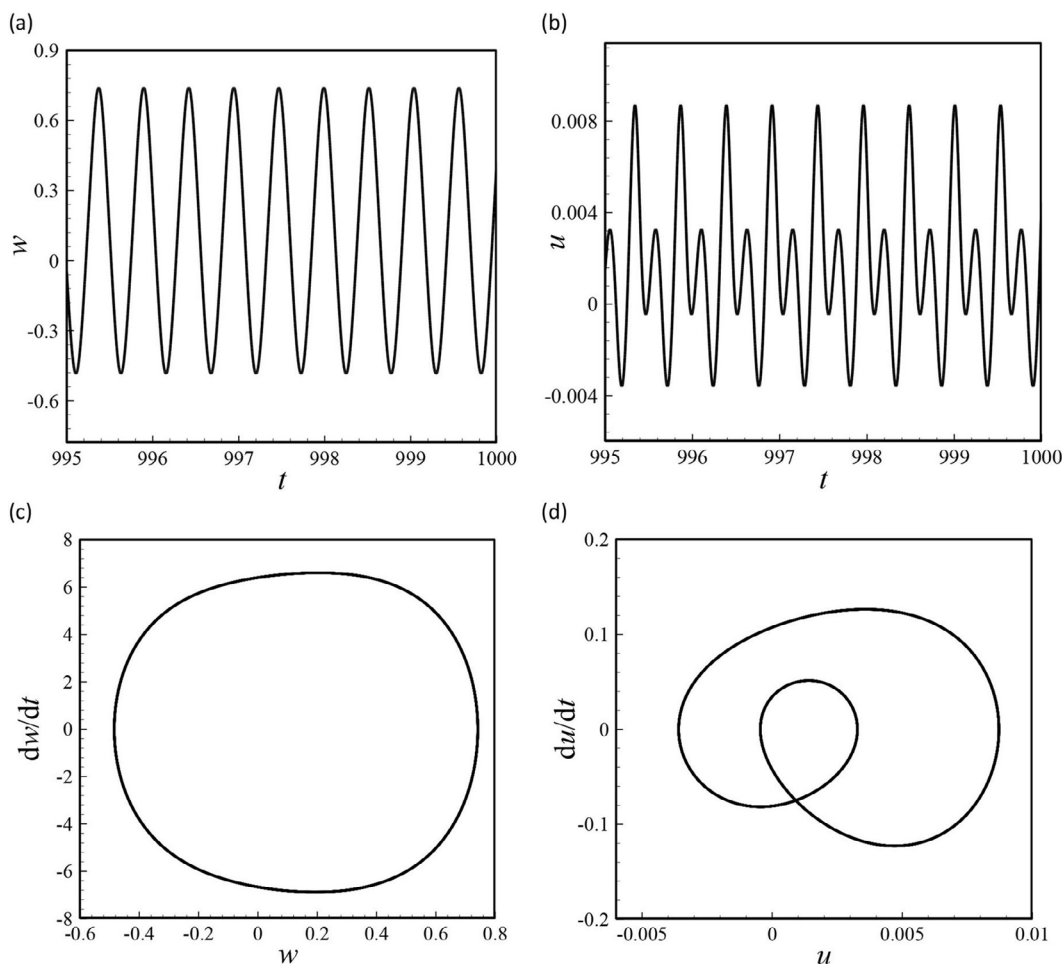
Fig. 6. Response of the tube in fig. 5 at $U_0=4.60$ for $A_0 = 0.05$, $\omega_f = 12.00$, and $U_1 = 0.10U_0$: (a) and (c) time history and phase-plane for $w[x = 0.5]$, respectively; (b) and (d) time history and phase-plane for $u[x = 0.65]$, respectively.

While maintaining all the other parameters constant, ω_f is increased to 24, twice of the original system, and the bifurcation response is plotted in fig. 8. The transverse motion shows a similar trend as shown in fig. 1 till $U_0 = 4.06$. However, in the longitudinal direction, the tube moves in the negative direction. In the transverse direction, a period-2 motion is seen after $U_0 = 4.06$ till $U_0 = 5.2$.
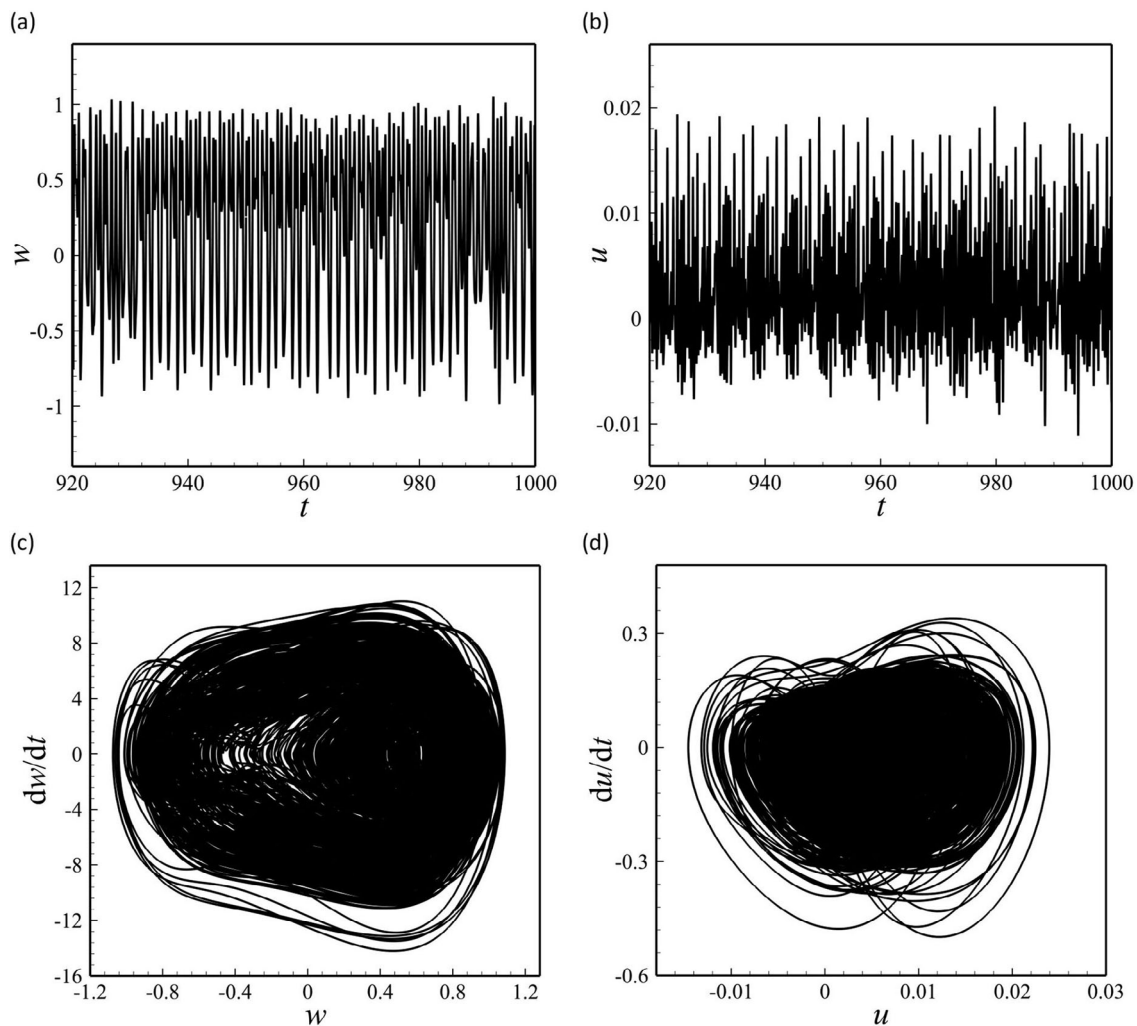
Fig. 7. Response of the tube in fig. 5 at $U_0 = 5.50$ for $A_0 = 0.05$, $\omega_f = 12.00$, and $U_1 = 0.10U_0$: (a) and (c) time history and phase-plane for $w[x = 0.5]$, respectively; (b) and (d) time history and phase-plane for $u[x = 0.65]$, respectively.

Indicated in fig. 9 is the size-dependent responses of perfectly straight viscoelastic nanotubes conveying pulsatile fluid with mean speed of $U_0 = 5.10$ for displacements along both transverse and longitudinal directions. The transverse motion is taken at displacement $x = 0.5$ while the axial motion is taken at $x = 0.65$. Furthermore, as this nanotube is perfectly straight, the geometrical imperfection amplitude is zero. The frequency of the nanotube is determined as $\omega_1 = 1.8886$. From fig. 9, it is evident that if the amplitude of flow speed grows, the nanotube experiences different motion kinds involving period-k ($k = 1, 2, 3, 6$) together with chaotic motion.

Figure 10 illustrates the bifurcation response of initially imperfect nanofluid-conveying viscoelastic nanotubes with geometrical imperfection amplitude, $A_0 = 0.005$. The mean speed, U_0 and the fundamental natural frequency ω_1 are 5.10 and 5.2407, respectively. It is observed that the nanotube undergoes the same motion type at the same amplitude for both transverse and longitudinal motions despite having different displacements. For small velocity amplitudes ($U_1 \leq 0.008$), the coupled behaviour is of period-1. By further increasing amplitude, the transverse and longitudinal motion types observed include period-2, period-4 and period-6. Beyond $U_1 = 0.28$, only period-2 motions are observed for the coupled motions. It is important to note that no complicated response is observed in fig. 10. The detailed motions of the nanotube of fig. 10 at $U_1 = 0.20$ is given in fig. 11. At this point, the system response is of period-4.

Furthermore, to investigate the effects of geometrical imperfection on the nanofluid-conveying viscoelastic nanotube, fig. 12 is plotted. This figure shows the bifurcation response of the viscoelastic nanotube for displacements in the transverse direction when $A_0 = 0.05$ and $A_0 = 0.15$. The point of displacement, mean speed and frequency ratio are $x = 0.5$, $U_0 = 5.10$ and $\omega/\omega_1 = 2.0$, respectively. When geometrical imperfection amplitude is $A_0 = 0.05$, period-1 motion type is seen for small amplitudes of fluid speed. For large values of U_1, it is observed that the transverse motion experiences a period-2 response. As the geometrical defect rises to $A_0 = 0.15$, the transverse motion is observed to undergo large amplitudes.
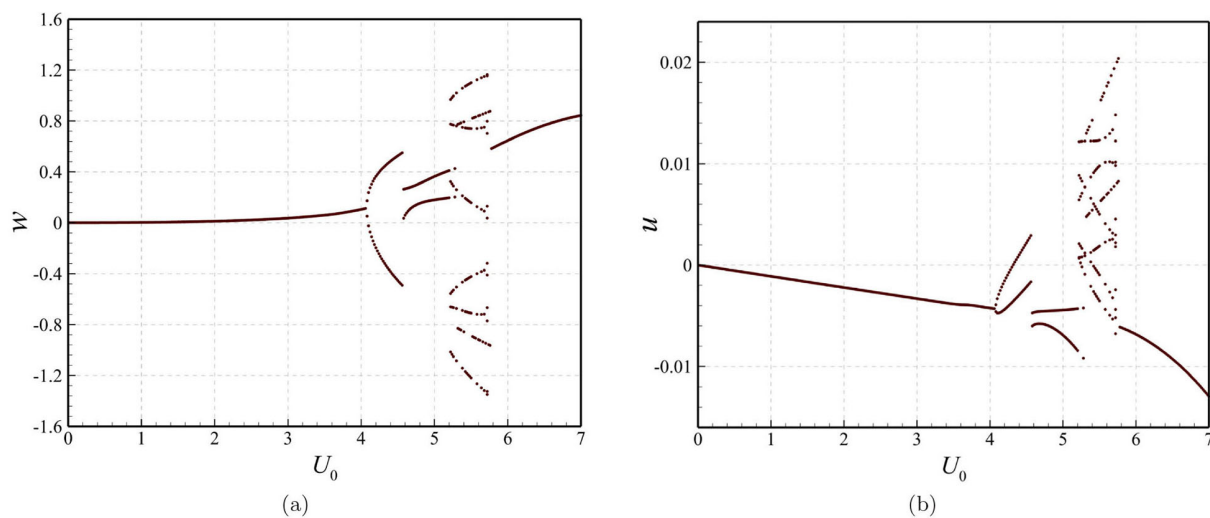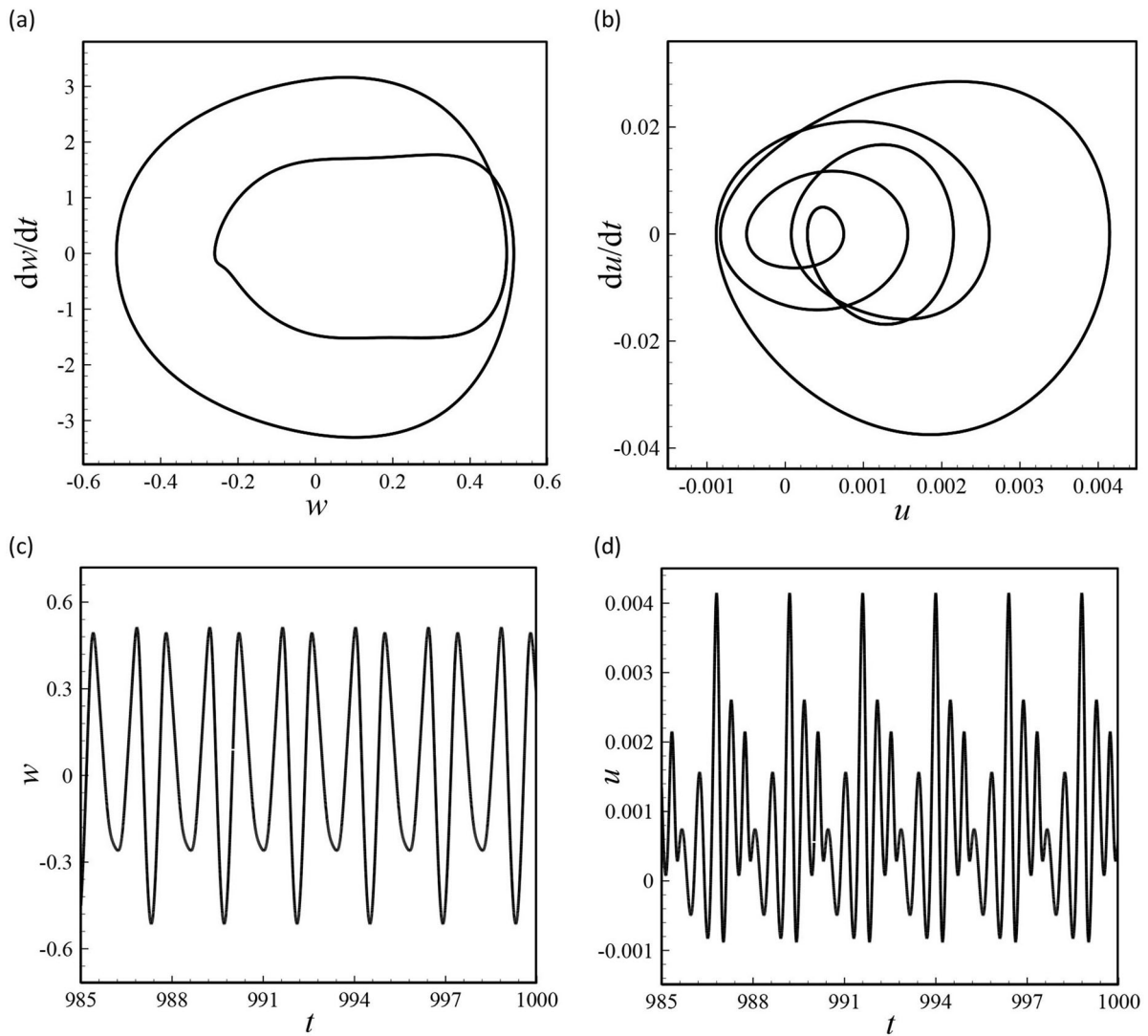
Fig. 8. Bifurcation response of initially imperfect nanofluid-conveying viscoelastic nanotubes for $A_0 = 0.05$, $\omega_f = 24.00$, and $U_1 = 0.10U_0$: (a) $w[x = 0.50]$; (b) $u[x = 0.65]$.
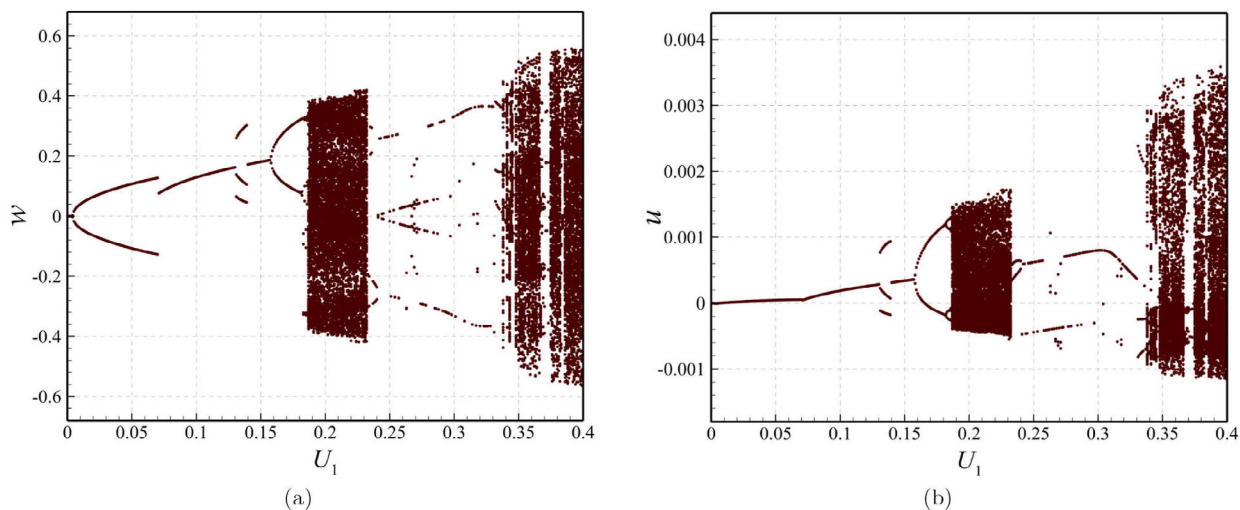

Fig. 9. Bifurcation response of perfectly straight nanofluid-conveying viscoelastic nanotubes for $U_0 = 5.10$, $A_0 = 0$, $\omega_1 = 1.8886$, and $\omega/\omega_1 = 2.0$: (a) $w[x = 0.50]$; (b) $u[x = 0.65]$.
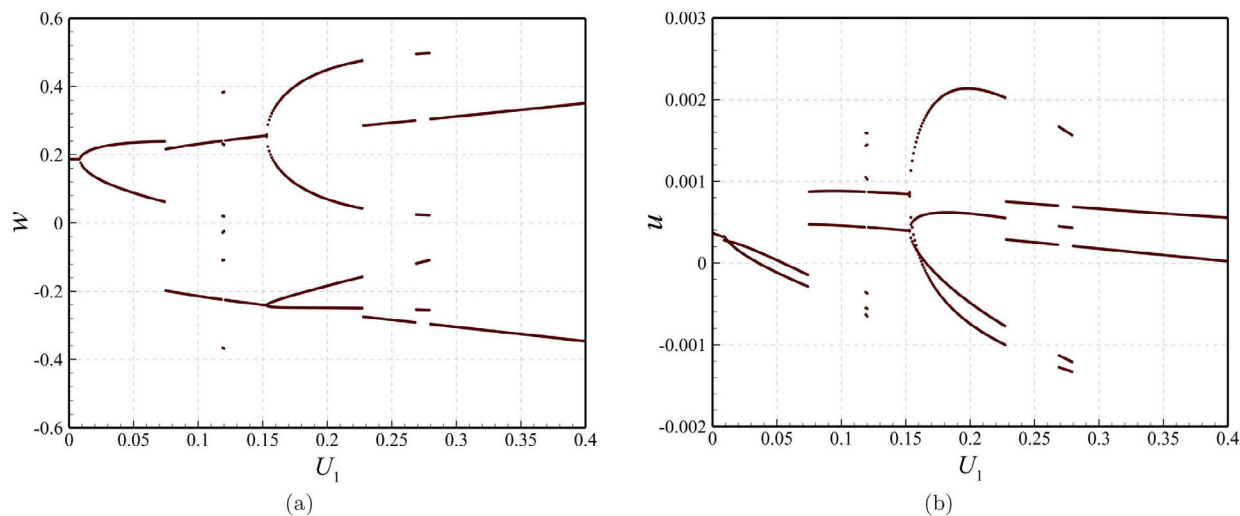
Fig. 10. Bifurcation response of initially imperfect nanofluid-conveying viscoelastic nanotubes for $U_0 = 5.10$, $A_0 = 0.005$, $\omega_1 = 5.2407$, and $\omega/\omega_1 = 2.0$: (a) $w[x = 0.50]$; (b) $u[x = 0.65]$.

Fig. 11. Period-4 response of the tube in fig. 10 at $U_1 = 0.20$ for $U_0 = 5.10$, $A_0 = 0.005$, $\omega_1 = 5.2407$, and $\omega/\omega_1 = 2.0$: (a) and (c) phase-plane and time trace for $w[x = 0.5]$, respectively; (b) and (d) phase-plane and time trace for $u[x = 0.65]$, respectively.
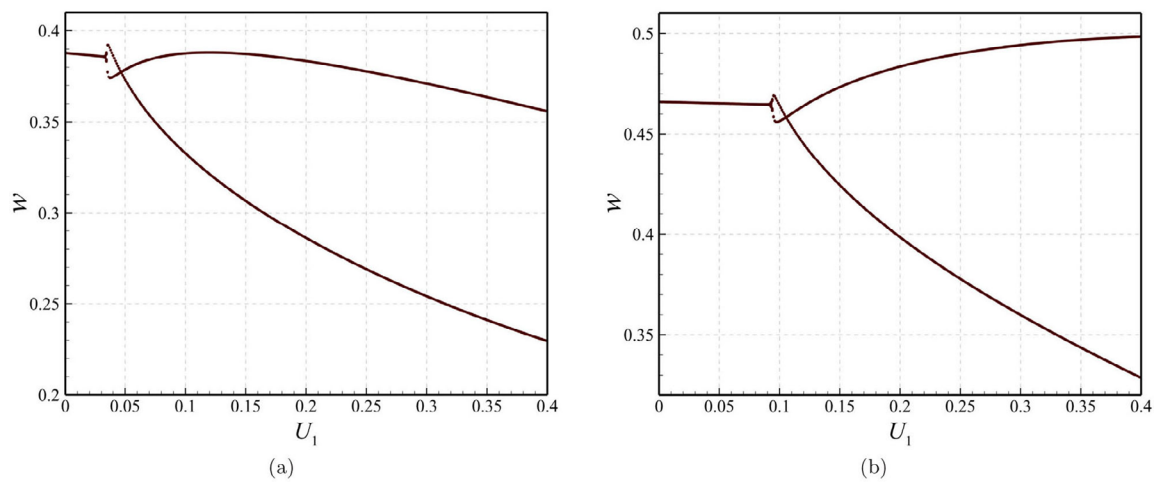
Fig. 12. Bifurcation response of initially imperfect nanofluid-conveying viscoelastic nanotubes; (a) $w[x = 0.5]$ when $U_0 = 5.10$, $A_0 = 0.05$, $\omega_1 = 12.0047$, and $\omega/\omega_1 = 2.0$; (b) $w[x = 0.5]$ when $U_0 = 5.10$, $A_0 = 0.15$, $\omega_1 = 17.9556$, and $\omega/\omega_1 = 2.0$.

6 Conclusions

The bifurcation response of viscoelastic imperfect nanotubes conveying pulsatile fluid was investigated in this article. A scale-dependent nonlinear fluid-structure interaction model was utilised to explore the bifurcations of imperfect nanotubes conveying flow. The model was developed using nonlocal strain gradient theory, Beskok-Karniadakis theory, Kelvin-Voigt method, Euler-Bernoulli theory and Hamilton's principle. Viscoelastic features were assumed for the solid part of the nanosystem. Coriolis and centrifugal accelerations and imperfection effects were factored in the model used. It was concluded that imperfections in nanotubes, the velocity and frequency of pulsatile flow all significantly affect the bifurcation response along transverse and longitudinal directions. The viscoelastic imperfect nanotube shows a period-1 motion when the pulsatile fluid has a low velocity. However, when the nanofluid exceeds a certain speed, numerous different motions are observed, from period-1 and period-3 to a chaotic behaviour. Changing the imperfection of nanotubes changes the chaos pattern. Compared to perfect nanotubes, imperfect nanotubes exhibit less chaos, and even none in some cases. In general, a nanosystem with higher U_0 or U_1 shows more chaos.

Author contribution statement

Oscar Zi Shao Ong and Kelly Yee have contributed equally to this work.

References

1. R.H. Baughman, C. Cui, A.A. Zakhidov, Z. Iqbal, J.N. Barisci, G.M. Spinks *et al.*, Science **284**, 1340 (1999).
2. A. Bachtold, P. Hadley, T. Nakanishi, C. Dekker, Science **294**, 1317 (2001).
3. S. Joseph, N. Aluru, Nano Lett. **8**, 452 (2008).
4. M. Longhurst, N. Quirke, Nano Lett. **7**, 3324 (2007).
5. N. Moldovan, K.-H. Kim, H.D. Espinosa, J. Microelectromech. Syst. **15**, 204 (2006).
6. M. Kamali, M. Shamsi, A. Saidi, Eur. Phys. J. Plus **133**, 110 (2018).
7. M.M. Adeli, A. Hadi, M. Hosseini, H.H. Gorgani, Eur. Phys. J. Plus **132**, 393 (2017).
8. A. Hadi, M.Z. Nejad, M. Hosseini, Int. J. Eng. Sci. **128**, 12 (2018).
9. M. Farajpour, A. Shahidi, F. Tabataba'i-Nasab, A. Farajpour, Eur. Phys. J. Plus **133**, 219 (2018).
10. F. Ebrahimi, M.R. Barati, P. Haghi, Eur. Phys. J. Plus **131**, 383 (2016).
11. M.F. Oskouie, R. Ansari, H. Rouhi, Eur. Phys. J. Plus **133**, 336 (2018).
12. A. Farajpour, M.H. Ghayesh, H. Farokhi, Int. J. Eng. Sci. **133**, 231 (2018).
13. M.H. Ghayesh, A. Farajpour, Int. J. Eng. Sci. **137**, 8 (2019).
14. H. Farokhi, M.H. Ghayesh, Commun. Nonlinear Sci. Numer. Simul. **59**, 592 (2018).
15. L. Panda, R. Kar, J. Sound Vib. **309**, 375 (2008).
16. A. Bajaj, Dyn. Stab. Syst. **2**, 19 (1987).
17. N.S. Namachchivaya, W. Tien, J. Fluids Struct. **3**, 609 (1989).
18. D. Gorman, J. Reese, Y. Zhang, J. Sound Vib. **230**, 379 (2000).
19. J. Łuczko, A. Czerwiński, J. Fluids Struct. **70**, 235 (2017).
20. M. Asghari, M. Ahmadian, M. Kahrobaiyan, M. Rahaeifard, Mater. Des. **31**, 2324 (2010).
21. L.-L. Ke, Y.-S. Wang, Compos. Struct. **93**, 342 (2011).
22. M. Salamat-talab, F. Shahabi, A. Assadi, Appl. Math. Model. **37**, 507 (2013).
23. M. Farajpour, A. Shahidi, A. Farajpour, Mater. Res. Express **5**, 035026 (2018).
24. H. Farokhi, M.H. Ghayesh, Int. J. Eng. Sci. **123**, 197 (2018).
25. M.H. Ghayesh, H. Farokhi, Int. J. Eng. Sci. **86**, 60 (2015).
26. M.H. Ghayesh, H. Farokhi, A. Gholipour, M. Tavallaeinejad, Int. J. Eng. Sci. **122**, 56 (2018).
27. A. Gholipour, H. Farokhi, M.H. Ghayesh, Nonlinear Dyn. **79**, 1771 (2015).
28. T.-Z. Yang, S. Ji, X.-D. Yang, B. Fang, Int. J. Eng. Sci. **76**, 47 (2014).
29. S. Mashrouteh, M. Sadri, D. Younesian, E. Esmailzadeh, Nonlinear Dyn. **85**, 1007 (2016).
30. M.H. Ghayesh, Microsyst. Technol. **24**, 1743 (2018).
31. H. Farokhi, M.H. Ghayesh, Int. J. Eng. Sci. **127**, 127 (2018).
32. H. Farokhi, M.H. Ghayesh, A. Gholipour, S. Hussain, Int. J. Eng. Sci. **112**, 1 (2017).
33. H. Farokhi, M.H. Ghayesh, S. Hussain, Int. J. Eng. Sci. **106**, 29 (2016).
34. C. Thongyothee, S. Chucheepsakul, T. Li, Adv. Mater. Res. **747**, 257 (2013).
35. M. Ece, M. Aydogdu, Acta Mech. **190**, 185 (2007).
36. L. Wang, Physica E **41**, 1835 (2009).

37. H.-L. Lee, W.-J. Chang, J. Appl. Phys. **103**, 024302 (2008).
38. Y. Zhang, G. Liu, X. Xie, Phys. Rev. B **71**, 195404 (2005).
39. M. Farajpour, A. Shahidi, A. Hadi, A. Farajpour., Mech. Adv. Mater. Struct. **26**, 1469 (2019).
40. M. Farajpour, A. Shahidi, A. Farajpour., Eur. Phys. J. Plus **134**, 218 (2019).
41. L. Li, X. Li, Y. Hu, Int. J. Eng. Sci. **102**, 77 (2016).
42. M. Şimşek, Int. J. Eng. Sci. **105**, 12 (2016).
43. L. Li, Y. Hu, Comput. Mater. Sci. **112**, 282 (2016).
44. M.H. Ghayesh, H. Farokhi, A. Farajpour, Eur. Phys. J. Plus **134**, 179 (2019).
45. A. Farajpour, M.H. Ghayesh, H. Farokhi, Int. J. Mech. Sci. **150**, 510 (2019).
46. H.-L. Lee, W.-J. Chang, Physica E **41**, 529 (2009).
47. M. Rafiei, S.R. Mohebpour, F. Daneshmand, Physica E **44**, 1372 (2012).
48. A. Farajpour, A. Rastgoo, M. Farajpour, Compos. Struct. **180**, 179 (2017).
49. H. Askari, E. Esmailzadeh, Compos. Part B: Eng. **113**, 31 (2017).
50. W. Xia, L. Wang, Comput. Mater. Sci. **49**, 99 (2010).
51. F. Liang, Y. Su, Appl. Math. Model. **37**, 6821 (2013).
52. M.H. Ghayesh, Int. J. Mech. Sci. **140**, 339 (2018).
53. M.H. Ghayesh, Int. J. Eng. Sci. **124**, 115 (2018).
54. M.H. Ghayesh, H. Farokhi, A. Gholipour, Int. J. Eng. Sci. **110**, 35 (2017).
55. M.H. Ghayesh, H. Farokhi, A. Gholipour, Int. J. Mech. Sci. **122**, 370 (2017).
56. H. Farokhi, M.H. Ghayesh, Int. J. Eng. Sci. **99**, 39 (2016).
57. H. Farokhi, M.H. Ghayesh, Int. J. Mech. Mater. Des. **13**, 43 (2017).